Electronic Supplementary Material (ESI) for Dalton Transactions

Photo-induced oxidation of [Fe^{II}(N4Py)CH_3CN] and related complexes

Apparao Draksharapu, Qian Li, Gerard Roelfes* and Wesley R. Browne*

Electronic Supporting Information

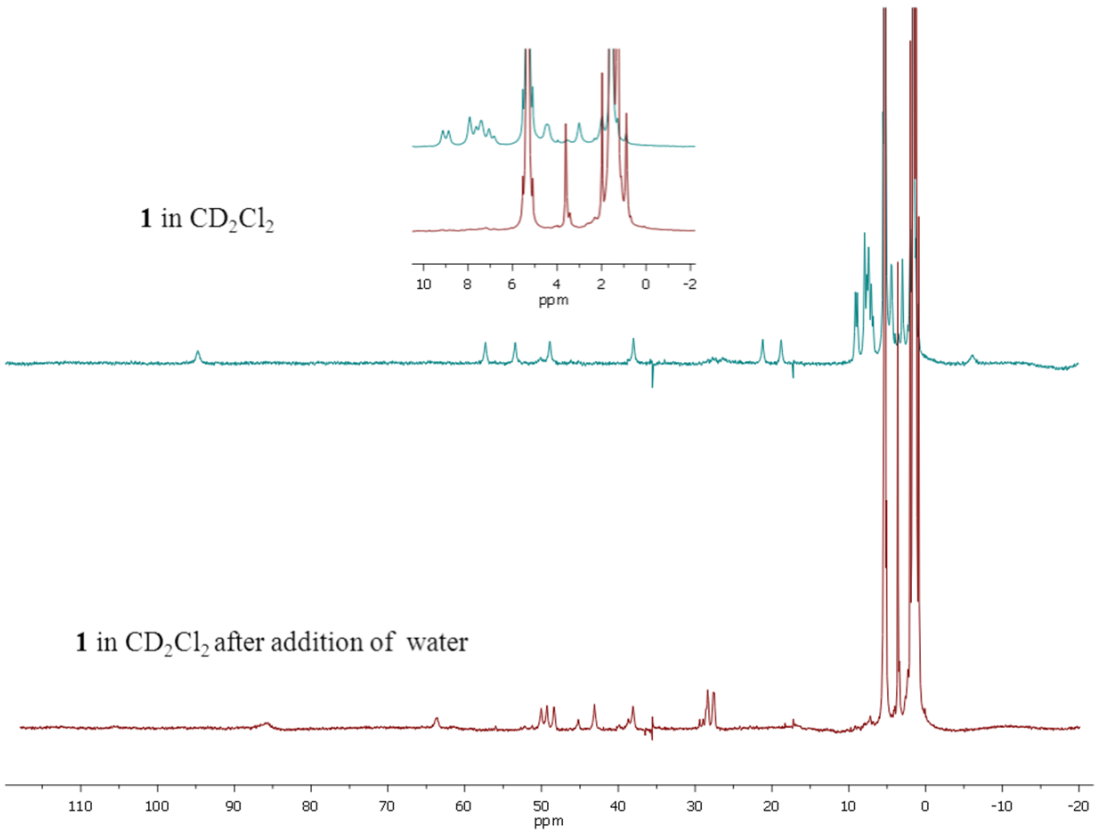

Fig. S1 ^{1}H NMR spectra of **1** in CD_2Cl_2 before and after saturation with water.

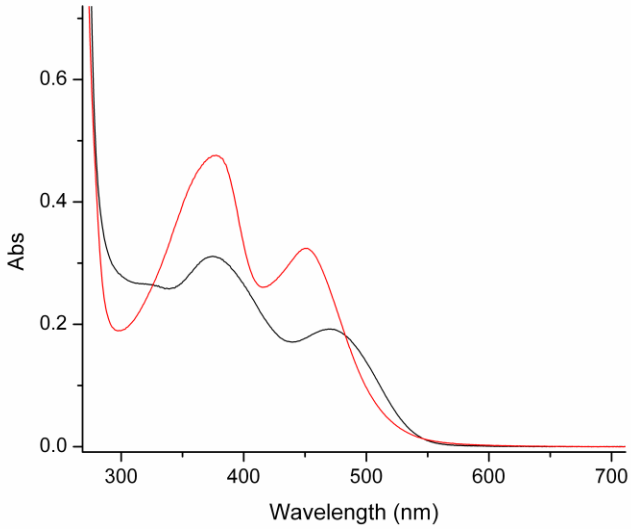

Fig. S2 UV/Vis spectra of **1** in CH_2Cl_2 before (red) and after (black) saturation with water.

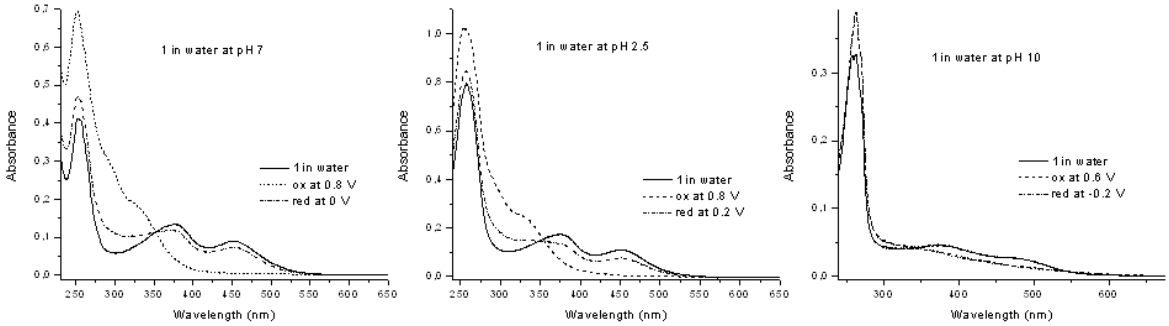

Fig. S3 Electrochemical oxidation of **1** and subseqent reduction at indicated potentials vs Ag/AgCl in 0.1 M KNO_3 at pH 7, 2.5 and 10.

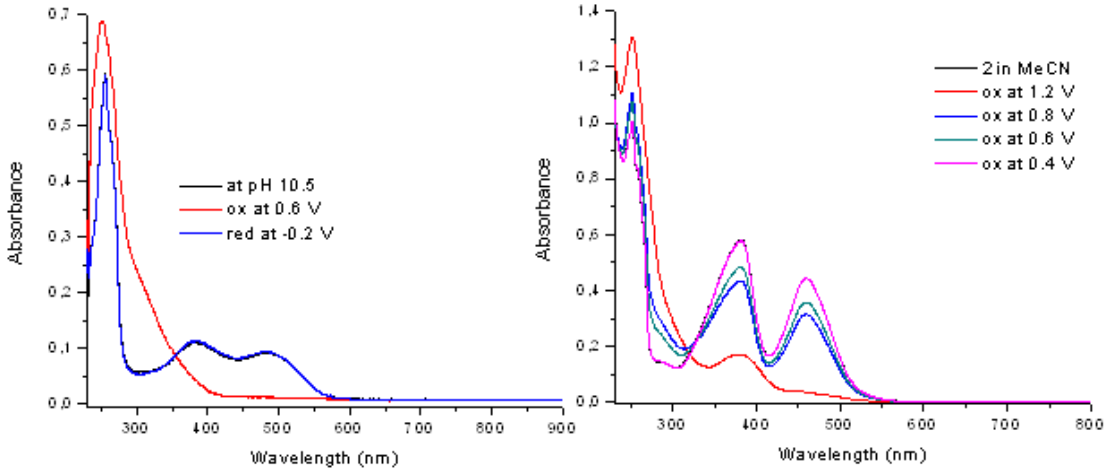

Fig. S4 Electrochemical oxidation of **2** (left) at 0.6 V and subseqent reduction at -0.2 V vs Ag/AgCl in 0.1 M KNO_3 at pH 10.5 and (right) at 1.2 V and subsequent reduction at 0.4 V in acetonitrile (0.1 M TBAPF-$_6$).

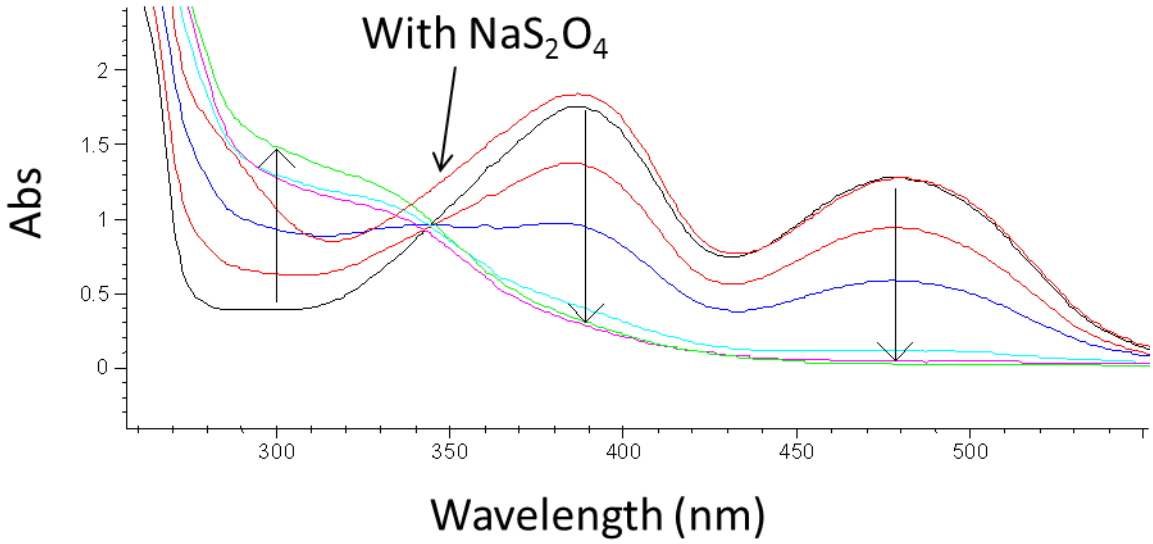

Fig. S5 Change in UV/Vis absorption spectra of **2** in water at pH 2 upon successive additions of Ce(IV)SO_4 and subsequently with $Na_2S_2O_4$.

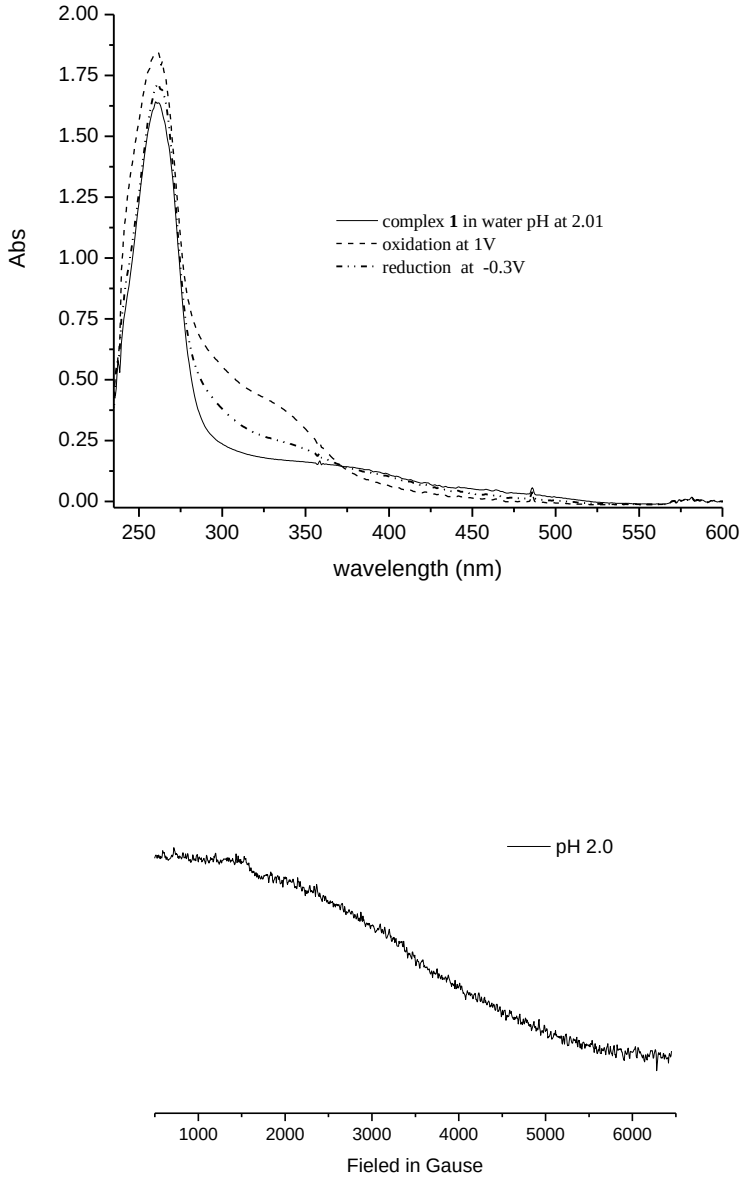

Fig. S6 UV/Vis spectroelectrochemistry and *ex-situ* EPR spectrum of **1** in H_2O at pH 2.0 upon oxidation at 1 V and reduction at -0.3 V vs Ag/AgCl in 0.1 M KNO_3. The EPR spectrum was recorded by freezing 0.2 ml of the solution from which the UV/Vis absorption spectrum at 1V was obtained.

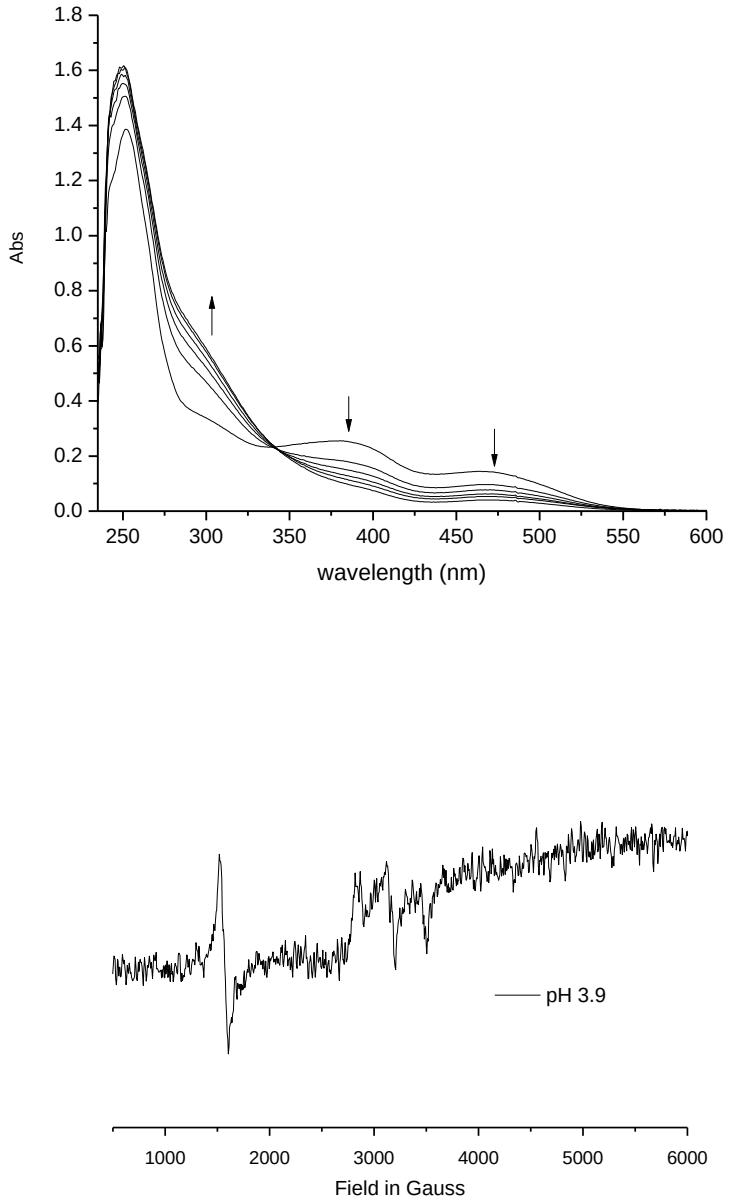

Fig. S7 UV/Vis spectroelectrochemistry and *ex-situ* EPR spectrum of **1** in H_2O at pH 3.9 oxidation at 0.6 V vs Ag/AgCl in 0.1 M KNO_3. The EPR spectrum was recorded by freezing 0.2 ml of the solution from which the UV/Vis absorption spectrum at 0.6 V was obtained.

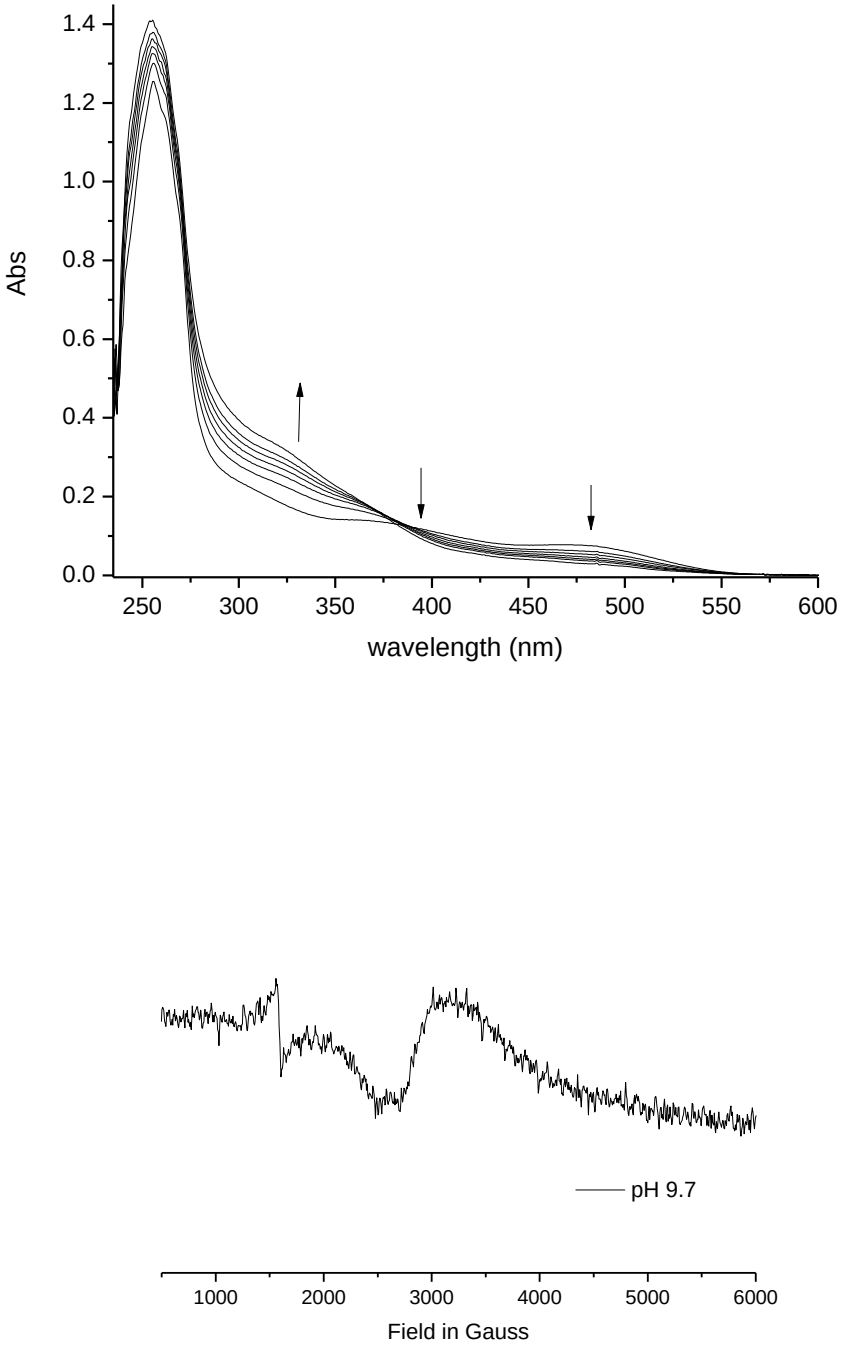

Fig. S8 UV/Vis spectroelectrochemistry and *ex-situ* EPR spectrum of **1** in H_2O at pH 9.7 oxidation at 0.6 V vs Ag/AgCl in 0.1 M KNO_3. Note that the signal at 3000 G is a spectral artefact. The EPR spectrum was recorded by freezing 0.2 ml of the solution from which the UV/Vis absorption spectrum at 0.6 V was obtained.

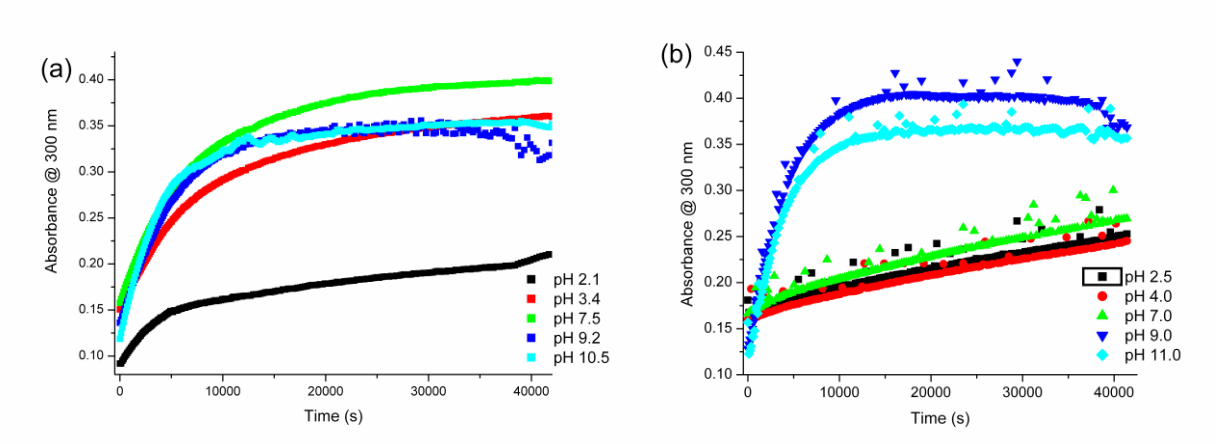

Fig. S9 Aerobic oxidation of (a) **1** and (b) **2** at in water various pHs.

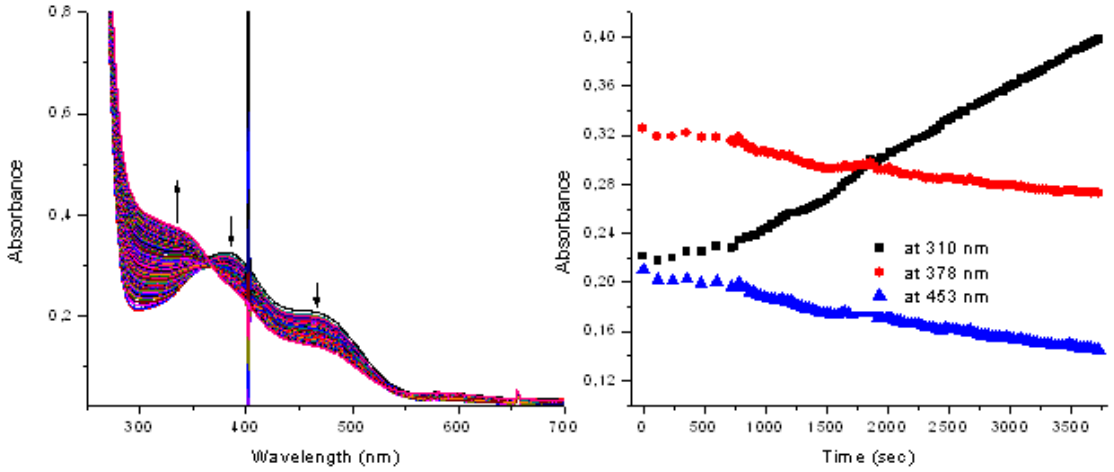

Fig S10. UV/Vis absorption spectra and spectral changes resulting from irradiation of **1** at λ_{ex} = 400 nm in water (left) absorption spectra over course of irradiation (right) time dependence of absorption at selected wavelengths. Irradiation starts at 750 s. The distortion in the spectra at 400 nm is due to scattered laser light.

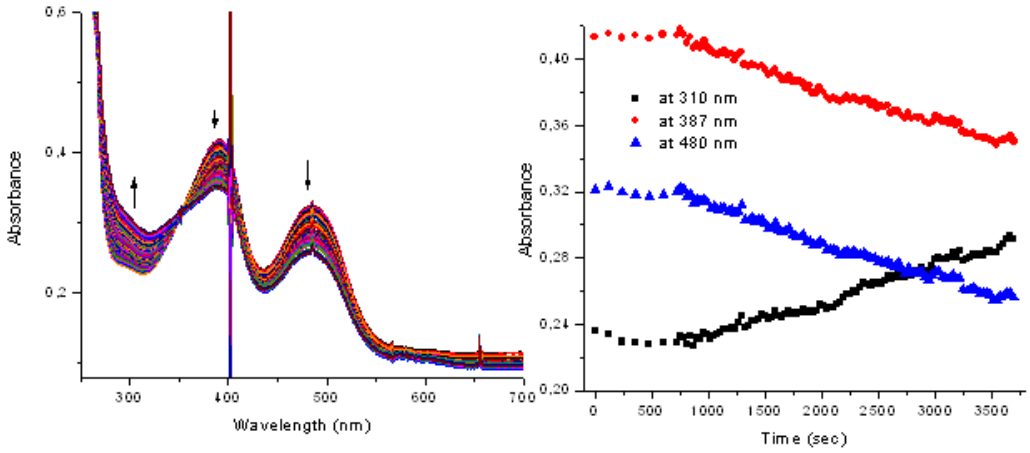

Fig S11. UV/Vis absorption spectra and spectral changes resulting from irradiation of **2** at λ_{ex} = 400 nm in water (left) absorption spectra over course of irradiation (right) time dependence of absorption at selected wavelengths. Irradiation starts at 750 s. The distortion in the spectra at 400 nm is due to scattered laser light.

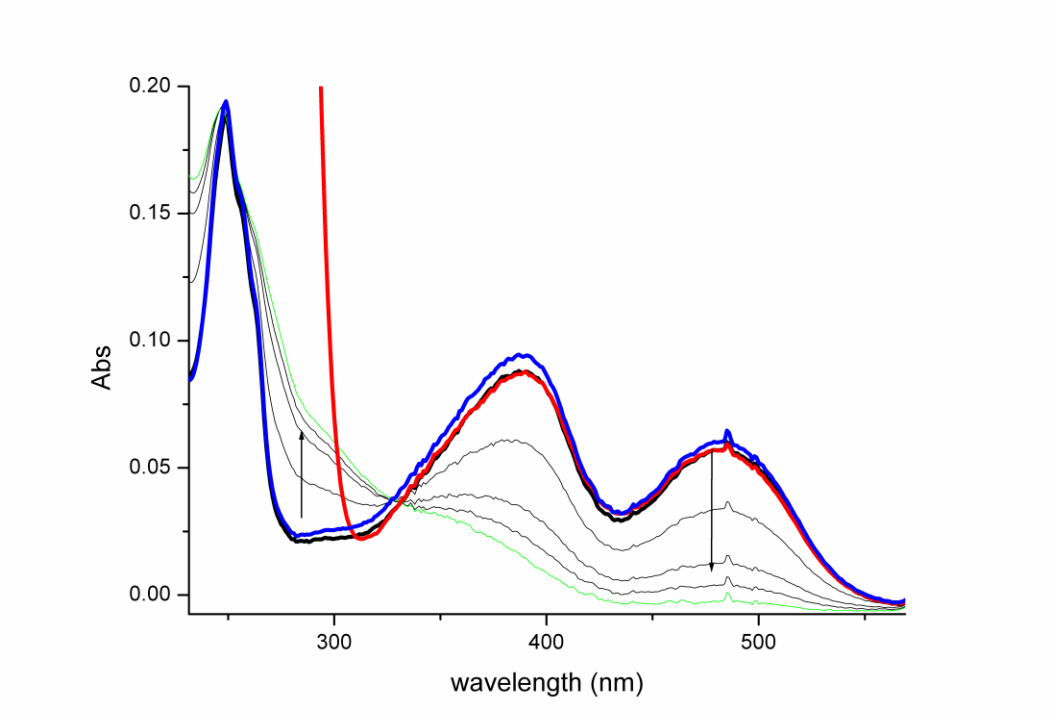

Fig S12. Changes observed in the UV/Vis absorption spectrum of **2** in at pH 5.6 upon oxidation with oxygen under irradiation at λ_{ex} = 365 nm. In blue is a sample held for the same period in the dark. In red is the spectrum after addition of ascorbic acid to the irradiated sample (green).

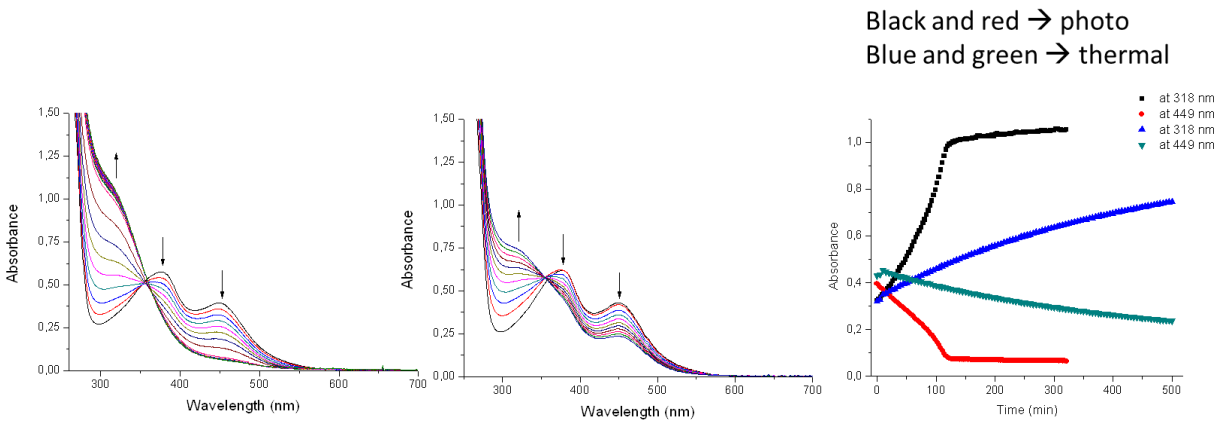

Fig S13. UV/Vis absorption spectra and spectral changes resulting from irradiation of **1** at λ_{ex} = 365 nm in methanol (left), changes in the absorption spectra with no irradiation (centre) and time dependence of absorption at selected wavelengths (right).

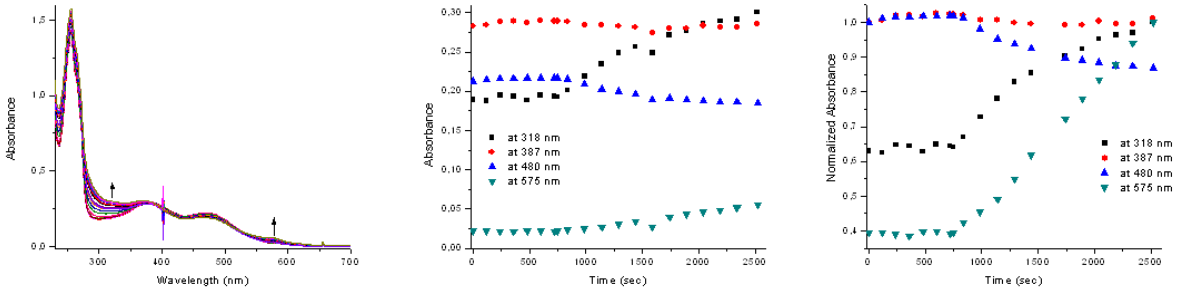

Fig S14. UV/Vis absorption spectra and spectral changes resulting from irradiation of **2** at λ_{ex} = 400 nm in methanol (left), time dependence of absorption at selected wavelengths not normalised (centre) and time dependence of absorption at selected wavelengths (right) normalised traces to show kinetics more clearly. Irradiation starts at 750 s. The distortion in the spectra at 400 nm is due to scattered laser light.

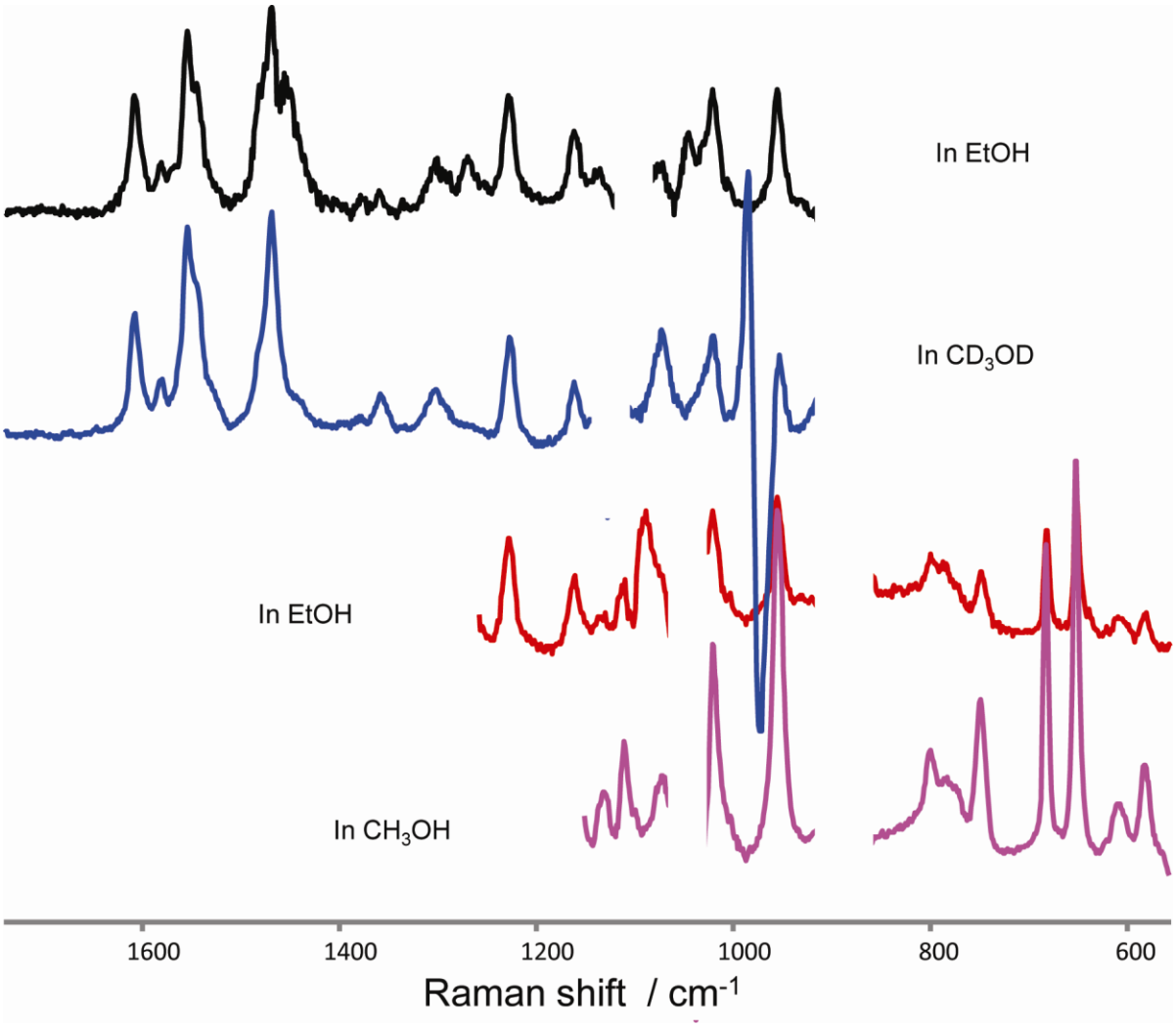

Fig. 15 Resonance Raman spectra of secondary product of **2** at λ_{ex} = 561 nm in methanol and ethanol. Solvent bands are masked by white boxes.